Available online at www.sciencedirect.com
SCIENCE DIRECT®
International Journal of Heat and Fluid Flow 25 (2004) 961–974
International Journal of HEAT AND FLUID FLOW
www.elsevier.com/locate/ijhff

Numerical and experimental investigation of turbulent characteristics in a drag-reducing flow with surfactant additives

Bo Yu [a,b], Fengchen Li [a,b], Yasuo Kawaguchi [a,*]

[a] Turbomachinery Research Group, Institute for Energy Utilization, National Institute of Advanced Industrial Science and Technology, 1-2 Namiki, Tsukuba, Ibaraki 305-8564, Japan
[b] Center for Smart Control of Turbulence, National Maritime Research Institute, 6-38-1, Shinkawa, Mitaka-shi, Tokyo 181-0004, Japan

Received 7 October 2003; accepted 16 February 2004
Available online 20 May 2004

Abstract

Cetyltrimethyl ammonium chloride (CTAC) surfactant additives, because of their long-life characteristics, can be used as promising drag-reducers in district heating and cooling systems. In the present study we performed both numerical and experimental tests for a 75 ppm CTAC surfactant drag-reducing channel flow. A two-component PIV system was used to measure the instantaneous streamwise and wall-normal velocity components. A Giesekus constitutive equation was adopted to model the extra stress due to the surfactant additives, with the constitutive parameters being determined by well-fitting apparent shear viscosities, as measured by an Advanced Rheometric Expansion System (ARES) rheometer. In the numerical study, we connected the realistic rheological properties with the drag-reduction rate. This is different from previous numerical studies in which the model parameters were set artificially. By performing consistent comparisons between numerical and experimental results, we have obtained an insight into the mechanism of the additive-induced drag-reduction phenomena.

Our simulation showed that the addition of surfactant additives introduces several changes in turbulent flow characteristics: (1) In the viscous sublayer, the mean velocity gradient becomes gentler due to the viscoelastic forces introduced by the additives. The buffer layer becomes expanded and the slope of the velocity profile in the logarithmic layer increases. (2) The locations where the streamwise velocity fluctuation and Reynolds shear stress attain their maximum value shifted from the wall region to the bulk flow region. (3) The root-mean-square velocity fluctuations in the wall-normal direction decrease for the drag-reducing flow. (4) The Reynolds shear stress decreases dramatically and the deficit of the Reynolds shear stress is mainly compensated by the viscoelastic shear stress. (5) The turbulent production becomes much smaller and its peak-value position moves toward the bulk flow region. All of these findings agree qualitatively with experimental measurements.

Regarding flow visualization, the violent streamwise vortices in the near wall region become dramatically suppressed, indicating that the additives weaken the ejection and sweeping motion, and thereby inhibit the generation of turbulence. The reduction in turbulence is accomplished by additive-introduced viscoelastic stress. Surfactant additives have dual effects on frictional drag: (1) introduce viscoelastic shear stress, which increases frictional drag; and (2) dampen the turbulent vortical structures, decrease the turbulent shear stress, and then decrease the frictional drag. Since the second effect is greater than the first one, drag-reduction occurs.

Keywords: Channel flow; DNS; Drag-reduction; Giesekus model; CTAC surfactant solution

1. Introduction

'Toms Effect,' named after its discoverer (Toms, 1948), occurs where the addition of a minute amount of a long-chain polymer into a liquid such as water can significantly reduce turbulent friction drag. This phenomenon is useful for reducing energy consumption, increasing flow rate, and decreasing the size of pumps, etc. in turbulent pipe flow systems. One of the most successful applications of drag-reducers has been in the Trans-Alaska Pipeline, where the desired discharge of an additional million barrels of crude oil per day was

* Corresponding author. Fax: +81-29-8617275.
E-mail addresses: yubobox@hotmail.com (B. Yu), lifch-ri@aist.go.jp (F. Li), kawaguchi.y@aist.go.jp (Y. Kawaguchi).

0142-727X/$ - see front matter © 2004 Elsevier Inc. All rights reserved.
doi:10.1016/j.ijheatfluidflow.2004.02.029

Nomenclature

c	conformation tensor
C	mean conformation tensor
C_f	friction factor $= 2\tau_w/\rho U_b^2$
h	half-height of the channel
p	pressure
P	mean pressure
q	general turbulent quantity
Re_b	Reynolds number $= 2\rho U_b h/\eta_s$
Re_τ	Reynolds number $= \rho U_\tau h/\eta_s$
R_{uu}	two-point correlation coefficient
t	time
u	velocity
U	mean velocity
U_b	mean bulk velocity
U_τ	friction velocity $= \sqrt{\tau_w/\rho}$
We_τ	Weissenberg number $= \rho\lambda U_\tau^2/\eta_s$
x_1, x	streamwise direction
x_2, y	wall-normal direction
x_3, z	spanwise direction

Greeks

α	mobility factor
β	ratio $= \eta_a/\eta_s$
$\dot{\varepsilon}$	extensional rate
$\dot{\gamma}$	shear rate
η_a	dynamic shear viscosity of surfactant contribution
η_s	dynamic shear viscosity of solvent contribution
η_0	shear viscosity of the surfactant solution at zero-shear rate $= \eta_a + \eta_s$
λ	relaxation time
ρ	density
ν	kinematic viscosity
τ	viscoelastic shear stress
τ_w	statistically averaged wall shear stress

Superscripts and subscripts

$(\ )'$	fluctuating component
$(\ )^+$	normalized by U_τ, ρ and η_s
$(\ )^*$	non-dimensional coordinate
$(\ )_{rms}$	root-mean-square fluctuations

accomplished by the addition of polymers rather than by constructing additional pumping stations. Motivated by an understanding of the Toms Effect, drag-reducers have been applied to save energy, and many drag-reducing additives have been found so far. Generally, all of the additives can be classified into three groups: (1) fiber, (2) polymer, and (3) surfactant. In the past 30 years, extensive studies have been carried out for the drag-reduction of polymer solutions. Their effectiveness, however, is often degraded by mechanical and thermal effects, which lead to irreversible changes in polymer structures with the elapse of time. The degradation of a polymer's effectiveness can make them unsuitable for circulation systems. Surfactant additives also suffer from temporary mechanical and thermal degradations, but they have the capability to 'repair' themselves in the order of seconds. They are the most promising agents for reducing the pumping power needed in district heating and cooling systems. Although surfactant additives have an advantage for circulation systems, in contrast to polymer solutions, investigations into the characteristics of the heat and flow in the drag-reduction caused by surfactant additives have only been performed in recent years. Our research group is motivated by the promising applications of surfactant additives and is carrying out both experimental and numerical tests to study the mechanism of additive-induced drag-reduction.

In a review of the literature, the mechanism of additive-induced drag-reduction has not been clearly described. For polymer solutions, two theoretical explanations are given. One was proposed by Lumley (1969, 1973), who postulated that the increased extensional viscosity due to the stretching of randomly coiled polymers tends to dampen the small eddies in the buffer layer and thicken the buffer layer, to give rise to the drag-reduction. Lumley emphasized that drag-reduction occurs only when the relaxation time of the solution is larger than the characteristic time scale of the turbulent flow. The other important theory was proposed by De Gennes (1990), who criticized the earlier scenario that used extensional viscosity, and argued that the elastic energy stored in the macromolecules causes drag-reduction. For surfactant solutions, generally, the super-order network structures made up of rod-like micelles show elasticity, and cause drag-reduction. Nevertheless, these explanations are qualitative. Recently, direct numerical simulation (DNS) has been used to quantitatively analyze the turbulence transport mechanism. With DNS, the instantaneous flow structures near the wall can be calculated accurately, which are difficult to measure precisely in experiments. The instantaneous extra stress associated with the deformation of macromolecules/network structures can be calculated which has not yet been directly measured in experimental conditions. The quantitative data obtained by DNS are helpful in analyzing the mechanism of drag-reduction. Moreover, in contrast to experiments, the effects of various physical properties can be easily isolated and studied by numerical simulations.

Main conclusions drawn from previous DNSs on the drag-reducing flow caused by additives are summarized below. Orlandi (1995) and DenToonder et al. (1997) carried out DNS using extensional viscosity models for a channel, and a pipe flow, respectively. Their results qualitatively agree with most experimental observations. Nevertheless, the inelastic characteristic of such extensional models cannot examine the onset phenomenon, an important feature of drag-reducing flow caused by additives. Sureshkumar et al. (1997) and Dimitropoulos et al. (1998) performed direct numerical simulations for a fully developed turbulence channel flow by using viscoelastic models (the FENE-P and the Giesekus models), and verified Lumley's hypothesis that drag-reduction is primarily an effect of the extension of the polymer chains where the increase in the extensional viscosity leads to the inhibition of turbulence-generating events. They also proposed a criterion for the onset of the drag-reduction. Angelis et al. (2002) further confirmed the ability of the FENE-P model to reproduce most of the essential effects of polymers in dilute solutions on the wall turbulence. Min et al. (2001) studied the role of elastic energy in turbulence drag-reduction caused by polymer additives using an elastic Oldroyd-B model. Yu and Kawaguchi (2003) studied the effect of the Weissenberg number on the turbulence flow structure using a Giesekus model.

All of the above studies using viscoelastic models (Sureshkumar et al., 1997; Dimitropoulos et al., 1998; Angelis et al., 2002; Min et al., 2001; Yu and Kawaguchi, 2003) show that the onset and drag-reduction rate are closely associated with relaxation and extensibility of macromolecule chain or network structures. In all of these numerical studies, however, the parameters in the constitutive equations were set artificially, so that comparisons made between the numerical and experimental results did not exactly correspond. Suzuki et al. (2001) attempted to use the model parameters that were well-fitted to the apparent shear viscosities to calculate the drag-reducing flow of a surfactant solution, but did not find drag-reduction. In the present study, we carried out both experimental and numerical studies for a turbulent channel flow of the 75 ppm CTAC solution. A Giesekus constitutive equation was used to calculate the extra stress caused by the surfactant additives and model parameters were obtained by well-fitting the measured shear viscosities of the 75 ppm CTAC surfactant solution. Hence, in the numerical part of the present investigation, we directly connect realistic rheological properties (such as relaxation time, and extensibility of the network structure in the surfactant solution) with the drag-reduction rate. Our objective is to understand the mechanism of the additive-induced drag-reduction by directly comparing the numerical analysis and experimental measurements.

2. Experimental

2.1. Surfactant solution

The surfactant solution used in the present study was cetyltrimethyl ammonium chloride (CTAC) dissolved in tap water with a concentration 75 ppm. Sodium salicylate was added to the solution to provide counter-ions with a weight concentration equivalent to that of CTAC. CTAC surfactant is effective in drag-reduction at temperatures ranging from 10 to 40 °C. The experimental measurements were carried out at a constant solution temperature of 30 °C.

2.2. Test loop

We used PIV equipment to measure the flow characteristics. The PIV measurement system consisted of a double pulse laser, laser sheet optics, CCD camera, timing circuit, PC and software. The details of the arrangement of the PIV system and the measurement procedure are described by Kawaguchi et al. (2002). Fig. 1 schematically shows the closed loop flow facility used in the present experiment, in which the pump drives fluids through the storage tank, the contraction of the filter, and the test channel and diffuser in circulation.

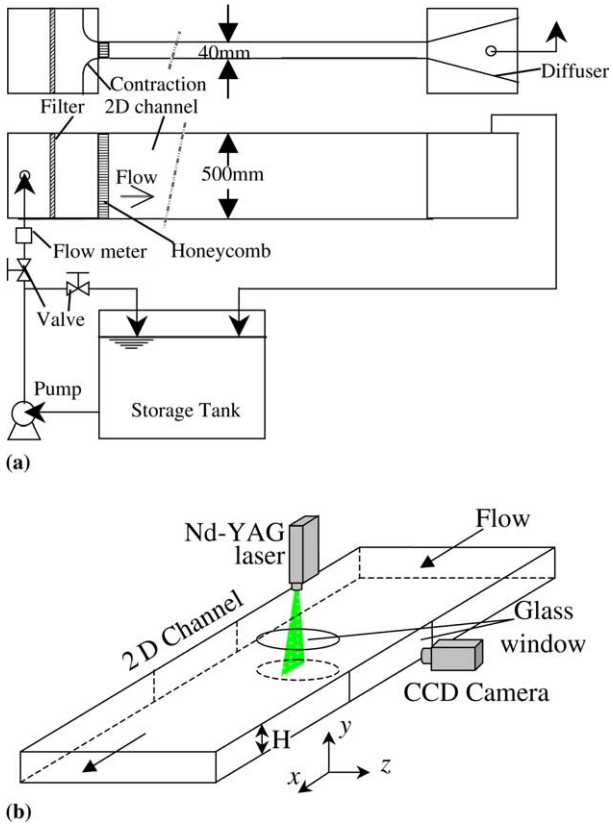

Fig. 1. Schematic diagram of the fluid loop and PIV measurement: (a) fluid loop and (b) two-component PIV measurement.

The channel is 0.04 m high, 0.5 m wide, and 10 m long (inside measurement). To remove large eddies, a honeycomb of 0.15 m length was employed at the entrance of the test section. The flow rate and pressure drops were measured by an electromagnetic flow meter with an uncertainty of 1.67×10^{-4} m^3/s and a precise pressure gauge. Experiments were carried out at $Re_b = 11,350$ for the CTAC solution.

3. Numerical procedure

The composition of the surfactant solution is more complicated than the polymer solution. Due to its complexity, no constitutive equations have been developed to describe the surfactant solution until now. Fortunately, the rheological properties of the surfactant solution are similar to those of the polymer solution despite the different microstructures, both of which show shear-thinning, and extensional thickening. Therefore, the models developed for the polymer solutions may be used to deal with the surfactant system. The apparent shear viscosities and extensional viscosities of the CTAC surfactant solution were measured with an Advanced Rheometric Expansion System (ARES) rheometer and an RFX instrument, respectively. The Giesekus model was able to qualitatively describe the measured shear viscosities and extensional viscosities (Kawaguchi et al., 2003). Applying the Giesekus model, the governing equations for dynamic motion of the surfactant solution are:

Continuity equation:

$$\frac{\partial u_i}{\partial x_i} = 0 \tag{1}$$

Momentum equation:

$$\rho\left(\frac{\partial u_i}{\partial t} + u_j\frac{\partial u_i}{\partial x_j}\right) = -\frac{\partial p}{\partial x_i} + \eta_s\frac{\partial}{\partial x_j}\left(\frac{\partial u_i}{\partial x_j}\right) + \frac{\partial \tau_{ij}}{\partial x_j} \tag{2}$$

Constitutive equation:

$$\tau_{ij} + \lambda\left(\frac{\partial \tau_{ij}}{\partial t} + \frac{\partial u_m\tau_{ij}}{\partial x_m} - \frac{\partial u_i}{\partial x_m}\tau_{mj} - \frac{\partial u_j}{\partial x_m}\tau_{mi} + \frac{\alpha}{\eta}\tau_{im}\tau_{mj}\right) = \eta_a\left(\frac{\partial u_i}{\partial x_j} + \frac{\partial u_j}{\partial x_i}\right) \tag{3}$$

where λ and α are, respectively, the relaxation time and the mobility factor. η_s and η_a are solvent and additive contributions to the zero-shear rate solution viscosity.

For steady, simple shear flow and extensional flow, the apparent shear viscosity and extensional viscosity may be analytically derived as

$$\eta = \eta_s + \eta_a\frac{4(1-\alpha)}{\sqrt{f+1}\left[\sqrt{f+1}+\sqrt{2}(1-2\alpha)\right]} \tag{4}$$

$$\eta_E = 3\eta_s + 3\eta_a \times \frac{3\lambda\dot{\varepsilon} + \sqrt{(1-2\lambda\dot{\varepsilon})^2 + 8\alpha\lambda\dot{\varepsilon}} - \sqrt{(1+\lambda\dot{\varepsilon})^2 - 4\alpha\lambda\dot{\varepsilon}}}{2\alpha\lambda\dot{\varepsilon}} \tag{5}$$

where

$$f = \sqrt{1 + 16\alpha(1-\alpha)\lambda^2\dot{\gamma}^2}$$

The RFX equipment, which employs two opposing nozzles to generate extensional flow, is currently the best instrument to measure extensional viscosity, but the error for a low concentration solution is large and the measured extensional viscosity is not sufficiently accurate to determine the numerical values of constitutive parameters. For this reason, the model parameters λ, η_a, and α in the constitutive equation (Eq. (3)) were determined by fitting reliable apparent shear viscosity data. The apparent shear viscosity was measured at the same temperature as in the experiments for drag-reduction. Fig. 2 shows the shear viscosities of a 75 ppm CTAC surfactant solution vs. shear rates, at a temperature of 30 °C, which are fitted to the curve of the Giesekus model with the parameters listed in the figure. The relaxation time λ, mobility factor α, and additive contribution to zero-shear-rate viscosity are 0.3 s, 0.005, and 3.2×10^{-3} Pa s, respectively. The viscosity of water at 30 °C is 8×10^{-4} Pa s, which contributes 20% to the zero-shear rate viscosity. The contribution of the additives to zero-shear-rate viscosity in the present study is large. Previous DNSs, reported by Dimitropoulos et al. (2001), Angelis et al. (2002) and Ptasinski et al. (2003) for polymer solutions, were made for low concentrations of polymer, and the ratio of the solvent viscosity to the zero shear-rate viscosity was usually artificially set to be 0.9. The contribution of the additives to zero-shear-rate viscosity is small. Hence, the shear-thinning in those studies was slight. From the present calculations, the contribution of surfactant additives is dominant in the zero shear-rate viscosity and the solution is apparently shear-thinning, as shown in Fig. 2.

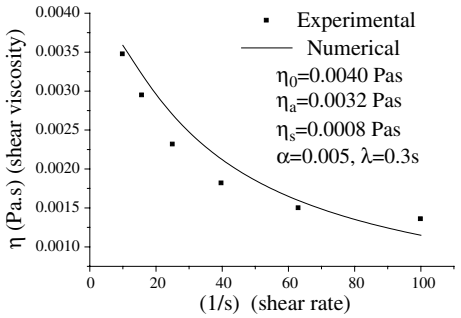

Fig. 2. Shear viscosity vs. shear rate.

By introducing the following non-dimensional variables:

$$x^* = \frac{x}{h}, \quad t^* = \frac{t}{h/U_\tau}, \quad u_i^+ = \frac{u_i}{U_\tau},$$

$$p^+ = \frac{p - P}{\rho U_\tau^2}, \quad c_{ij}^+ = \tau_{ij}\lambda/\eta_a + \delta_{ij} \tag{6}$$

The governing equations can be written in dimensionless forms as follows:

$$\frac{\partial u_i^+}{\partial x_i^*} = 0 \tag{7}$$

$$\frac{\partial u_i^+}{\partial t^*} + u_j^+ \frac{\partial u_i^+}{\partial x_j^*} = -\frac{\partial p^+}{\partial x_i^*} + \frac{1}{Re_\tau}\frac{\partial}{\partial x_j^*}\left(\frac{\partial u_i^+}{\partial x_j^*}\right) + \frac{\beta}{We_\tau}\frac{\partial c_{ij}^+}{\partial x_j^*} + \delta_{1i} \tag{8}$$

$$\frac{\partial c_{ij}^+}{\partial t^*} + \frac{\partial u_m^+ c_{ij}^+}{\partial x_m^*} - \frac{\partial u_i^+}{\partial x_m^*}c_{mj}^+ - \frac{\partial u_j^+}{\partial x_m^*}c_{mi}^+ + \frac{Re_\tau}{We_\tau}\left[c_{ij}^+ - \delta_{ij} + \alpha(c_{im}^+ - \delta_{im})(c_{mj}^+ - \delta_{mj})\right] = 0 \tag{9}$$

where p^+ is the excess hydrostatic pressure, δ_{1i} is the mean pressure gradient, and c_{ij}^+ is the conformation tensor associated with the deformation of the network structure formed by long, rod-like micelles in the surfactant solution. It also has a simple relationship with the extra stresses τ_{ij} as $\tau_{ij} = \eta_a/\lambda(c_{ij} - \delta_{ij})$, where the force $\eta/\lambda\delta_{ij}$ is a contribution from Brownian motion of surfactant particles. Four important non-dimensional parameters are used in the governing equations: Re_τ, We_τ, α and β. Re_τ ($Re_\tau = \rho U_\tau h/\eta_s$) is the frictional Reynolds number based on the frictional velocity and half of the channel height. We_τ ($We_\tau = \rho\lambda U_\tau^2/\eta_s$) is non-dimensional relaxation time. The mobility factor α indicates the extensibility of the network structures in the surfactant solution. β is a ratio defined as $\beta = \eta_a/\eta_s$, where η_a and η_s are the surfactant contribution and the solvent contribution to the zero-shear rate viscosity of the solution ($\eta_0 = \eta_a + \eta_s$), respectively. Note that the Reynolds number and the Weissenberg number are based on the viscosity of the solvent. A solvent-based Reynolds number, rather than a solution-based Reynolds number is adopted in the present study because it shows directly the overall effect of surfactant additives in relation to the solvent. This definition is useful for practical applications. By setting $\beta = 0$, the Navier–Stokes equation for a Newtonian fluid is recovered. A calculation was carried out for surfactant solutions at $Re_b = 12,080$ ($Re_\tau = 300$). The bulk Reynolds number is similar to that in the experiment ($Re_b = 11,350$). By using values of λ and η_a from the above, we have $We_\tau = 54$ and $\beta = 4$.

A computational box $10h \times 2h \times 5h$ in x, y and z directions was chosen. The computational domain in wall units (η_s, U_τ and ρ) is $3000\times600\times1500$. A grid system of $96\times128\times96$ (in x, y and z) meshes was adopted. Non-uniform grids in the wall-normal direction were used with grid-spacing of Δy^+ varying from about 0.45 next to the wall to 9 at the center. Uniform grids were used in the x and z directions and the corresponding grid-spacings were $\Delta x^+ = 31.3$ and $\Delta z^+ = 15.6$, respectively.

The periodic boundary conditions were imposed for both the streamwise (x-) and spanwise (z-) directions, while a non-slip condition was adopted for the top and bottom walls. Unlike the velocity component, the conformation components at the walls evolve over time and have values that are determined from Eq. (9) by setting the velocity components at the walls to equal zero. An instantaneous velocity field of a Newtonian fluid with a Reynolds number $Re_\tau = 150$ from our previous work (Yu and Kawaguchi, 2003) was adopted as the initial velocity field. The initial fields for pressure and conformation tensor were simply set as a zero field.

The computational algorithm is a fractional step method using the Adams–Bashforth scheme for the time advancement. For spatial discretization, a second-order finite difference scheme was employed. A high-resolution scheme, MINMOD, was used to make discrete the convective term in the constitutive equation to enhance the numerical stability (Yu and Kawaguchi, 2004). To avoid a zigzag pressure field, staggered grids were employed in which pressure and conformation components were stored at the cell center while velocity components were located at the cell borders.

4. Results

Ensemble averaging in the periodic direction and time were carried out to obtain statistical steady turbulent quantities:

$$\langle q \rangle = \frac{1}{N_x N_z N_t}\sum_0^{N_t}\sum_0^{N_x}\sum_0^{N_z} q(x,y,z,t) \tag{10}$$

In our simulation, flow reaches a steady state. Calculations were carried out for a further $6000\eta_s/\rho U_\tau^2$ and $2500\eta_s/\rho U_\tau^2$ time units for the surfactant solution and Newtonian flow for statistical averaging. To make the averages, 100 statistical independent fields were saved at equal intervals.

In the numerical simulation, the mean Reynolds numbers $Re_b = 12,080$ was calculated to be slightly larger than $Re_b = 11,350$, as measured in the experiment. Although we could adjust Re_τ in the calculations to make the mean Reynolds number almost the same as those in the experiments, this would be unnecessary

Table 1
Friction factor and drag-reduction rate for 75 ppm CTAC surfactant solution

Re_b	C_f	C_f^D	C_f^V	$DR\%$
12,080 (Numer.)	0.00493	0.00696	0.00248	29
11,350 (Exp.)	0.00346	0.00707	0.00258	51

since small variations in the Reynolds number only slightly alters turbulence characteristics such as the friction factor, root-mean-square velocity fluctuations, and the Reynolds shear stress. The Fanning friction factor was adopted to evaluate the friction coefficient. In Table 1, C_f was the measured or calculated friction factor, C_f^D was evaluated by Dean's correlation (Dean, 1978) and C_f^V is the limited friction factor asymptote (Virk et al., 1970). The drag-reduction rate is defined as the reduction of the friction factor with respect to the Newtonian fluid at an equal mean Reynolds number Re_b, i.e.:

$$DR\% = \frac{C_f^D - C_f}{C_f^D} \times 100\% \tag{11}$$

Table 1 shows that the measured drag-reduction rate of 51% is larger than the predicted value of 29%. Both the numerical and the experimental friction factors were larger than Virk's asymptotic friction factor (Virk et al., 1970).

For Newtonian fluid, we did calculation and experiment at $Re_b = 13,070$ ($Re_\tau = 380$) and $Re_b = 10,800$, respectively. The correctness of these results was checked by comparisons with values reported in the literature and these results are included for comparison with the surfactant solution.

Fig. 3 compares the mean streamwise velocity profiles of the fully developed turbulence flow of a Newtonian fluid with that of the CTAC solution, for which the well-known relationships of Newtonian fluids—linear law in the viscous sublayer $u^+ = y^+$, logarithmic law $u^+ = 2.5 \ln y^+ + 5.0$ in the inner layer, and Virk's asymptote velocity profile for the drag-reducing flow—are given for comparison. The numerical and measured mean velocity profiles of the Newtonian fluid are in good agreement with $u^+ = y^+$ in the viscous sublayer and with $u^+ = 2.5 \ln y^+ + 5.0$ in the logarithmic layer as shown in Fig. 3(a) and (b). Both calculated and experimental results show that the addition of surfactant additives dramatically decreases the mean velocity values as well as decreases their gradient in the viscous sublayer. The mean velocity profile of surfactant solution is also shifted upwards in the logarithmic layer with a steeper gradient than that of the Newtonian fluid, and a narrower logarithmic layer (a wider buffer layer) is established with the additives. Interestingly, the velocity profile of the surfactant solution (Fig. 3(b)) more closely approaches the Virk's asymptote velocity profile, compared to that shown in Fig. 3(a), which corresponds to a higher drag-reduction rate.

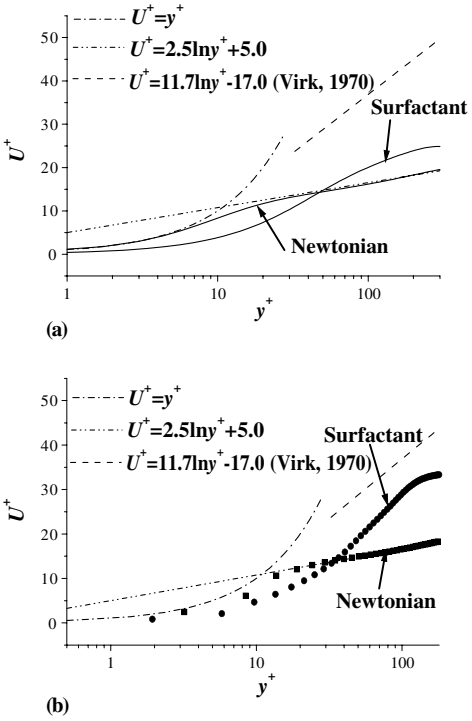

Fig. 3. Mean velocity profiles: (a) numerical and (b) experimental.

From Fig. 3, the linear relationship $u^+ = y^+$ is clearly not satisfied if the wall scales are based on the viscosity of the solvent. An effective dynamic viscosity may be introduced as follows:

$$\eta_{\text{eff}} = \frac{1 - \frac{y^+}{Re_\tau} - \left(-\overline{u'^+ v'^+}\right)}{\frac{\partial U^+}{\partial y^+}} \eta_s \tag{12}$$

The effective viscosity is shown in Fig. 4(a), where the effective viscosity is seen to be much larger than the solvent viscosity and increases with wall distance. By using the effective viscosity at the wall, the rescaled wall unit becomes $y^{+^*} = y^* Re_\tau^* = y^+ Re_\tau \eta_s / \eta_{\text{eff}}$. With the adoption of y^{+*}, $u^+ = y^{+*}$ is recovered in the vicinity of the wall, as shown in Fig. 4(b).

The root-mean-square velocity fluctuations obtained from the numerical simulations and the experiments are presented in Fig. 5(a) and (b), respectively. In Fig. 5(b), only two components (u_{rms}^+ and v_{rms}^+) are given because our PIV measurement is two-dimensional. Both the numerical and experimental results show that, with the addition of surfactant additives, the peak positions of the streamwise velocity fluctuation intensity u_{rms}^+ are located wider apart from the wall than those for the Newtonian flows. In the experiment, surfactant additives decrease u_{rms}^+, but in the numerical calculations, they increase it. For larger Reynolds number $Re_b = 3 \times 10^4$, and the experimental results show that

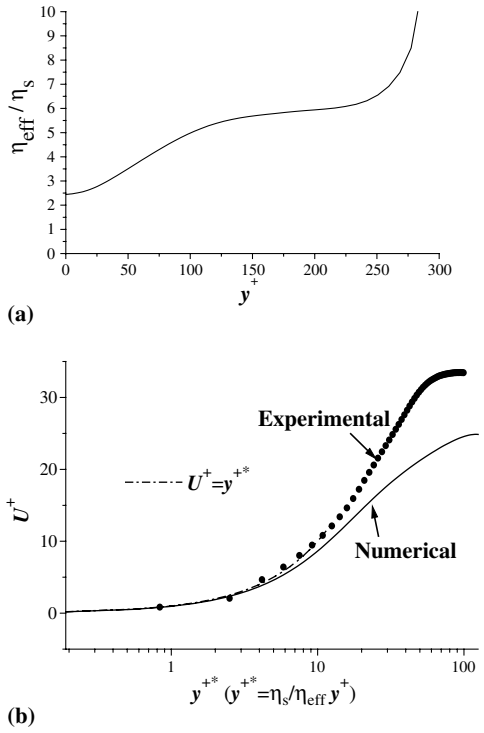

Fig. 4. Effective viscosity and velocity profile with respect to the rescaled wall-normal distance for surfactant solution: (a) effective viscosity and (b) mean velocity profile.

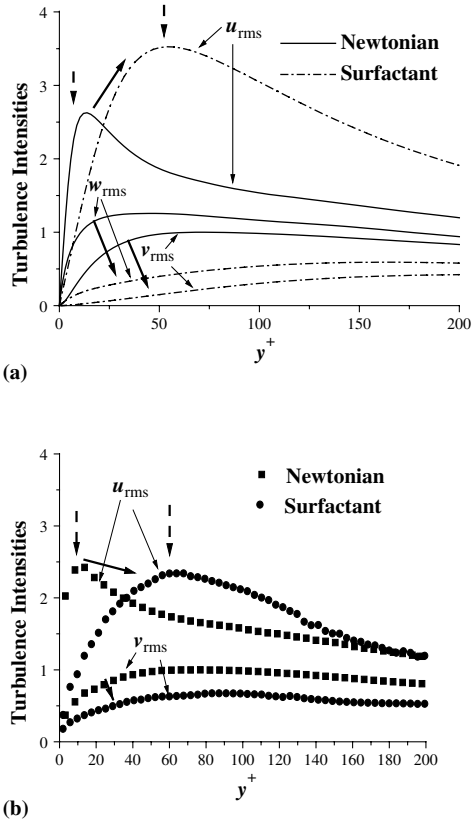

Fig. 5. Root-mean-square velocity fluctuations: (a) numerical and (b) experimental.

u^+_{rms} is enhanced compared to the Newtonian fluid. Thus, the decrease or increase of u^+_{rms} is not an essential feature of the drag-reducing flow caused by surfactant additives, while the shift of its peak-value position to the bulk flow is an essential feature, which is consistent with a wider buffer layer. Both the numerical calculations and the experiments show that v^+_{rms} decreases appreciably for the surfactant solution. A decrease in w^+_{rms}, by adding surfactant additives, is also seen in Fig. 5(a). The decrease in the velocity fluctuation intensities in the wall-normal and spanwise directions, as will be shown later, is due to the energy redistribution.

The total shear stress can be used to confirm if the calculation has reached a statistically steady state. When a steady state is reached, the following balance equation is satisfied:

$$\tau_{total} = 1 - \frac{y^+}{Re_\tau} = -\overline{u'^+ v'^+} + \frac{\partial U^+}{\partial y^+} + \beta \frac{C^+_{xy}}{We_\tau} \tag{13}$$

The last term on the right hand of Eq. (13) is the viscoelastic stress, which is equal to zero for the Newtonian fluid flow. The mean velocity gradient in the viscous sublayer that becomes gentler with the surfactant additives can be explained by Eq. (13). In the viscous sublayer, the Reynolds shear stress is negligible, due to the positive viscoelastic stress (as shown in Fig. 6), where the mean velocity gradient becomes smaller to satisfy the balance equation. By integration from the wall, the mean velocity must have values that are less than those of the Newtonian fluid.

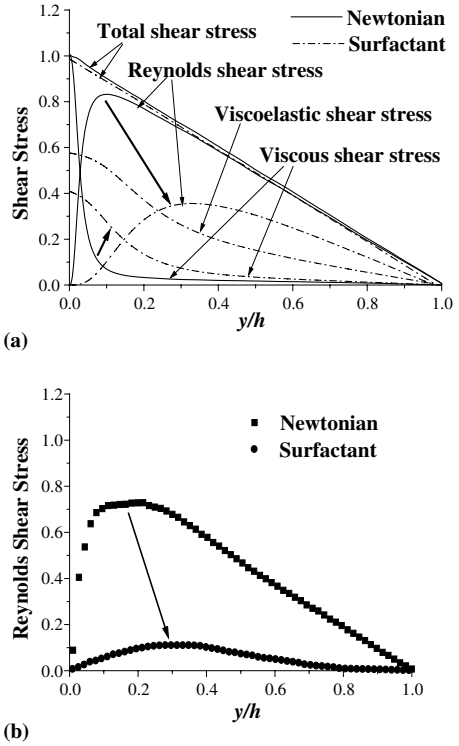

Fig. 6. Budget of shear stress: (a) numerical and (b) experimental.

Statistically steady states were confirmed for both the Newtonian fluid and the CTAC surfactant solution (Fig. 6(a)). Viscous shear stress is seen to increases appreciably, except for the decrease in the vicinity of the wall ($y^+ < 10$), with the addition of surfactant additives. The Reynolds shear stress decreases dramatically with its maximum value around half that of the Newtonian fluid, and the location where Reynolds shear stress reaches its maximum value shifts from the wall region to the bulk flow. The decrease of the Reynolds shear stress is due to the increase in the viscous shear stress and the positive contribution made by the viscoelastic shear stress, with a greater effect from the latter. The viscoelastic stress is the largest component in the near-wall region, where the Reynolds shear stress decreases most appreciably. The viscoelastic stress is about 50% of the total shear stress in the whole region of the channel, indicating that a small amount of additives greatly changes the balance of the stress budget. The decrease in the Reynolds shear stress was observed (Fig. 6(b)), and the measured Reynolds shear stresses were smaller than the predicted values.

Drag-reduction is often attributed to a decrease in the Reynolds shear stress. This explanation is somewhat crude, however, and from Eq. (13) and Fig. 6(a), besides the decrease in the Reynolds shear stress, a positive mean extra viscoelastic shear stress is induced that is associated with the deformation of network structure formed by the rod-like micelles of the surfactant solution. The presence of viscoelastic shear stress must introduce frictional drag and the frictional drag actually is derived from three components: viscous shear stress, Reynolds shear stress, and viscoelastic shear stress. To quantitatively identify the contributions made by each of these components to the friction factor, a twofold (double) integration is applied $\int_0^1 \int_0^y \mathrm{d}y^* \mathrm{d}y^*$ to Eq. (13). Transforming the multiple integration to a single integration is performed by applying the integration by parts, to obtain an integration expression for the friction factor,

$$C_f = \underbrace{12/Re_b}_{\text{viscous contribution}} + 6\int_0^1 \underbrace{\frac{\left(-\overline{u'^+v'^+}\right)(1-y^*)}{U_b^{+2}}}_{\text{turbulence contribution}} \mathrm{d}y^* + 6\int_0^1 \underbrace{\beta\frac{C_{xy}^+}{We_\tau U_b^{+2}}(1-y^*)}_{\text{viscoelastic contribution}} \mathrm{d}y^* \tag{14}$$

This integration was first proposed by Fukagata et al. (2002) (referred to as the FIK integration) to evaluate active turbulent control and we extend it to describe the drag-reducing flow caused by additives. The above equation shows that the friction factor is decomposed into a viscous contribution, which is identical to the laminar solution, the turbulence contribution, and the mean extra viscoelastic stress contribution. The turbulence contribution is proportional to the weighted average of the Reynolds shear stress, for which the weight linearly decreases with the distance from the wall. This fact quantitatively supports the observation for turbulent flow that turbulence structures that appear closer to the wall than the position of maximum Reynolds shear stress are more responsible for the frictional drag in wall turbulence. The viscoelastic contribution is also proportional to the weighted average viscoelastic shear stress with the weight decreasing linearly from 1 at the wall to zero at the center of the channel. For the Newtonian and viscoelastic flows, the fractional contribution made by each part is shown in Fig. 7(a). Apparently, at the same bulk Reynolds number, the absolute value of the viscous contribution is the same as that of the Newtonian fluid. Thus, the addition of surfactant additives dramatically decreases the turbulence contribution to friction drag, and introduces frictional drag by the viscoelastic contribution. Surfactant additives therefore have dual effects on frictional drag to: (1) introduce viscoelastic shear force, which has the function to increase frictional drag; and (2) dampen the turbulent vortical structures, to decrease turbulent shear stress and then decrease frictional drag. The drag-reduction occurs because the second effect exceeds that of the first. Fig. 7(b) shows the cumulative contributions made by the Reynolds shear stress and viscoelastic shear

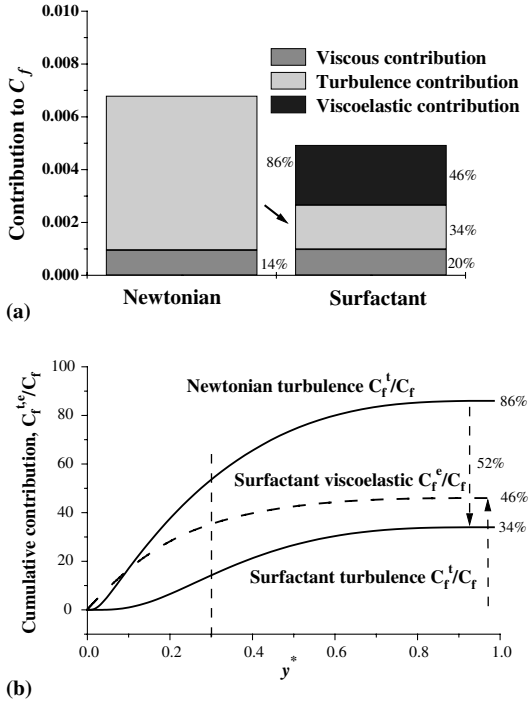

Fig. 7. Fractional contribution and cumulative contribution to friction factor in calculation case: (a) fractional contribution and (b) cumulative contribution.

stress. The decrease of the Reynolds shear stress contribution and the increase of the viscoelastic contributions occur primarily in the buffer layer.

The integrated balance equation for mean kinetic energy can be derived as follows:

$$\int_{-1}^{1} \underset{\text{I}}{\frac{U^+}{Re_\tau}}\mathrm{d}y^* = \int_{-1}^{1} \underset{\text{II}}{-\overline{u'^+v'^+}\frac{\partial U^+}{\partial y^+}}\mathrm{d}y^* + \int_{-1}^{1} \underset{\text{III}}{\frac{\mathrm{d}U^+}{\mathrm{d}y^+}\frac{\mathrm{d}U^+}{\mathrm{d}y^+}}\mathrm{d}y^* + \int_{-1}^{1} \underset{\text{IV}}{\frac{\beta}{We_\tau}C_{xy}^+\frac{\mathrm{d}U^+}{\mathrm{d}y^+}}\mathrm{d}y^* \tag{15}$$

The work done by the average pressure gradient (I) is equal to the work of deformation by the Reynolds shear stress (II) and the dissipation (III) of mean flow energy by viscosity (we name it viscous dissipation) and the work by mean viscoelastic stress (IV). For Newtonian flow, the last term at the right hand of Eq. (15) is zero.

The integrated balance equation for turbulent kinetic energy can be derived as follows:

$$\int_{-1}^{1} \underset{\text{II}}{-\overline{u'^+v'^+}\frac{\partial U^+}{\partial y^+}}dy^* = \int_{-1}^{1} \underset{\text{V}}{\overline{\left(\frac{\partial u_i'^+}{\partial x_k^+}\right)\left(\frac{\partial u_i'^+}{\partial x_k^+}\right)}}\mathrm{d}y^* + \int_{-1}^{1} \underset{\text{VI}}{\frac{\beta}{We_\tau}\left(\overline{c_{ik}'^+\frac{\partial u_i'^+}{\partial x_k^+}}\right)}\mathrm{d}y^* \tag{16}$$

For Newtonian flow, production of turbulence is lost by the dissipation due to the fluctuating velocity (V, we name it turbulent dissipation). With the addition of surfactant additives, turbulence is not only lost by turbulent dissipation but also through the effect of fluctuations in viscoelastic stress (VI).

The integrated balance equation for elastic energy can be derived as

$$0 = \int_{-1}^{1} \underset{\text{IV}}{\frac{\beta}{We_\tau}\frac{\partial U^+}{\partial y^+}C_{xy}^+}\mathrm{d}y^* + \int_{-1}^{1} \underset{\text{VI}}{\frac{\beta}{We_\tau}\overline{\frac{\partial u_i'^+}{\partial x_j^+}c_{ij}'^+}}\mathrm{d}y^* + \int_{-1}^{1} \underset{\text{VII}}{\frac{\beta}{2We_\tau^2}\left[(3-C_{ii}^+)-\alpha(C_{im}^+-\delta_{im})^2\right]}\mathrm{d}y^* \tag{17}$$

The last term (VII) of Eq. (17) is elastic dissipation. From Eqs. (15)–(17), the input energy by the mean pressure gradient is clearly seen to be dissipated by viscosity and elasticity. To identify the energy distribution quantitatively, each term in Eqs. (15)–(17) is calculated for both a Newtonian fluid and the surfactant solution. Their fractional contributions are listed in Fig. 8. Clearly, the energy transportation process for surfactant solution is quite different from that of the Newtonian fluid. The input energy by the mean pressure gradient is dissipated through Path 1 and Path 2. Path 1

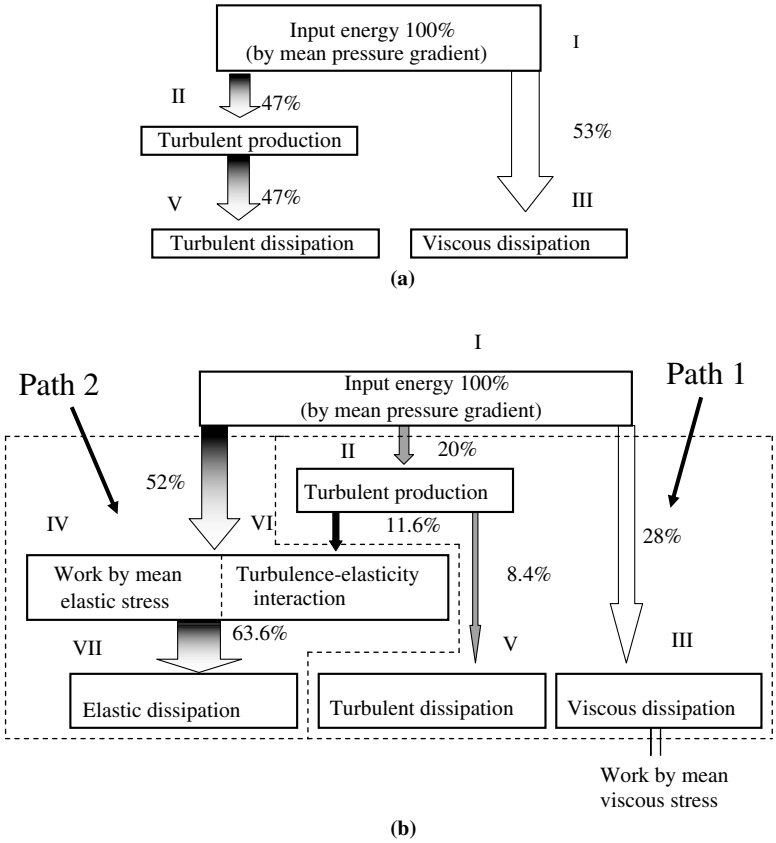

Fig. 8. Comparison of the energy transportation process for: (a) Newtonian flow and (b) surfactant solution.

is identical to the Newtonian case. One interaction is present between the two paths, namely, energy transport from turbulent production to a turbulence–elasticity interaction. Due to the addition of the surfactant additives, viscous dissipation becomes much smaller. Surfactant additives inhibit energy transfer to turbulent production and inhibit energy transfer to turbulent dissipation. Most of the energy is transferred to the work by the mean elastic stress and to the work by fluctuating elastic stress, and finally dissipated by the relaxation of the deformed network structure to its equilibrium state. The following equations present details of the energy budgets.

The budget terms of Reynolds stress $\overline{u_i'^+u_j'^+}$, in the fully developed channel flow field, can be expressed as

$$\frac{\mathrm{D}}{\mathrm{D}t}\left(\overline{u_i'^+u_j'^+}\right) = P_{ij} + T_{ij} + D_{ij} + \Pi_{ij} - \varepsilon_{ij} + E_{ij} \tag{18}$$

where the terms on the right-hand side of the above equation are identified as follows

$$P_{ij} = -\left(\overline{u_j'^+u_k'^+}\frac{\partial U_i^+}{\partial x_k^+} + \overline{u_i'^+u_k'^+}\frac{\partial U_j^+}{\partial x_k^+}\right) \qquad \text{production rate}$$

$$T_{ij}^R = -\frac{\partial}{\partial x_k^+}\left(\overline{u_i'^+u_j'^+u_k'^+}\right) \qquad \text{turbulent transport rate}$$

$$\Pi_{ij} = -\left(\overline{u_j'^+\frac{\partial p'^+}{\partial x_i^+}} + \overline{u_i'^+\frac{\partial p'^+}{\partial x_j^+}}\right) \qquad \text{vel.–press.-gradient term}$$

$$D_{ij} = \frac{\partial^2}{\partial x_k^{+2}}\left(\overline{u_i'^+u_j'^+}\right) \qquad \text{viscous diffusion rate}$$

$$\varepsilon_{ij} = \overline{2\left(\frac{\partial u_i'^+}{\partial x_k^+}\right)\left(\frac{\partial u_j'^+}{\partial x_k^+}\right)} \qquad \text{dissipation rate}$$

$$E_{ij} = \frac{\beta}{We_\tau}\left(\overline{u_i'^+\frac{\partial c_{jk}'^+}{\partial x_k^+}} + \overline{u_j'^+\frac{\partial c_{ik}'^+}{\partial x_k^+}}\right)$$

turbulence–elasticity interaction

In Eq. (18), as compared to Newtonian fluid, there is an extra term, called the turbulence–elasticity interaction. By setting $i = j$ in Eq. (18), summing the index i, and dividing the sum by 2, the balance equation of mean turbulent kinetic energy is obtained.

The budget terms of turbulent kinetic energy are plotted in Fig. 9 as a function of the dimensionless wall distance y^+ for both the Newtonian fluid and the CTAC surfactant solution. The production rates calculated by the measured instantaneous velocity fluctuations are also included for comparison. It is clearly seen that the magnitudes of the budget terms significantly decrease with the addition of surfactant additives. The positions, where production rate reaches its maximum value, molecular diffusion and turbulence diffusion reach their

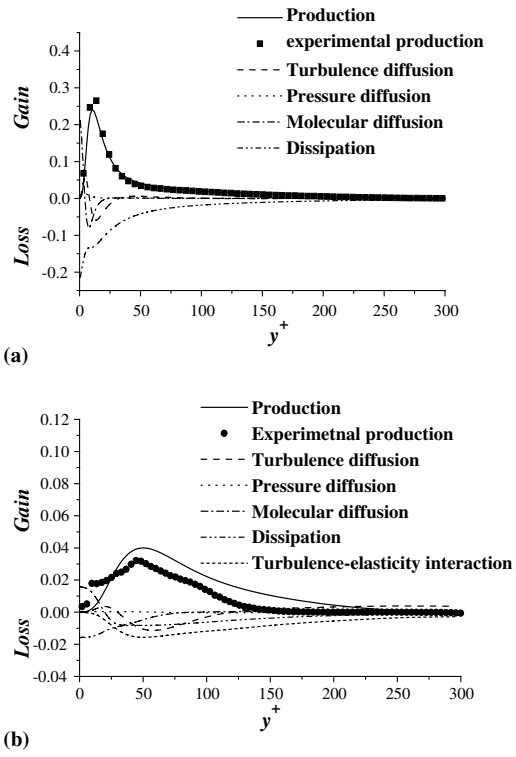

Fig. 9. Budget of turbulent kinetic energy: (a) Newtonian fluid and (b) surfactant solution.

minimum values, shift towards to the bulk flow region. For example, the peak value-position of the production rate shifts from $y^+ = 10$ to 50. These shifts are consistent with the expansion of the buffer layer. The maximum value of the production decreases by 83% as compared to Newtonian flow. This decrease must be due to the decrease of Reynolds shear stress. The wall friction factor is related to the turbulent production, as the turbulence level is decreased, the frictional drag also decreases. For Newtonian flow at $y^+ > 30$, the production term is balanced with the dissipation term. For the surfactant solution, however, the balancing is much more complicated. At $30 < y^+ < 100$, the production term becomes balanced with the sum of the turbulent diffusion, molecular diffusion, dissipation, and viscoelastic contribution terms. At $100 < y^+ < 150$, the production term is balanced with dissipation and turbulence–elasticity interaction terms. For $y^+ > 150$, the turbulent diffusion term becomes a large-gain term, and at the core region, is the largest producing term. At $y^+ > 250$, the turbulent diffusion term is balanced with the dissipation term and turbulence–elasticity interaction term. The turbulence–elasticity interaction acts as a strong sink-term along the channel height. Moreover, the negative peak position of the turbulence–elasticity interaction is almost the same as that of the production rate at $y^+ = 50$, which shows that the effect of the surfactant additives on turbulence flow is primarily in the buffer layer. Due to the strong

turbulence–elasticity interaction, the percentage decrease of the dissipation term is larger than that of the production rate. For example, its peak value decrease by 93%. Although the surfactant additives significantly change the values and distribution of the budget terms, the production, turbulent diffusion, molecular diffusion, and other terms show identical trends in variation for both the Newtonian fluid and surfactant solution, with the terms in the latter varying flatly. The measured production rates of the Newtonian fluid agree well with the numerical predictions except in the near-wall region, where the experimental values are larger. The agreement of the production rates of the CTAC surfactant solution between experimental and numerical calculations is qualitatively good.

The budget terms of the Reynolds normal stress $\overline{u'^+u'^+}$, $\overline{v'^+v'^+}$, and $\overline{w'^+w'^+}$ are shown in Figs. 10–12. The magnitude of all budget terms becomes smaller and their peak-value positions are located closer to the bulk flow than those of the Newtonian flow, due to the addition of surfactant additives. The decrease in amplitude of the budget terms of $\overline{v'^+v'^+}$ and $\overline{w'^+w'^+}$ are larger than those of $\overline{u'^+u'^+}$. The production rate of $\overline{u'^+u'^+}$ is twice that of the turbulent kinetic energy because production rates are zero for the normal component $\overline{v'^+v'^+}$ and the spanwise component $\overline{w'^+w'^+}$. For Newtonian flow, at $y^+ > 50$, one half of $\overline{u'^+u'^+}$ that is gained by production, is lost by the dissipation rate, whereas the other half is redistributed to $\overline{v'^+v'^+}$ and $\overline{w'^+w'^+}$ through the pressure strain correlation.

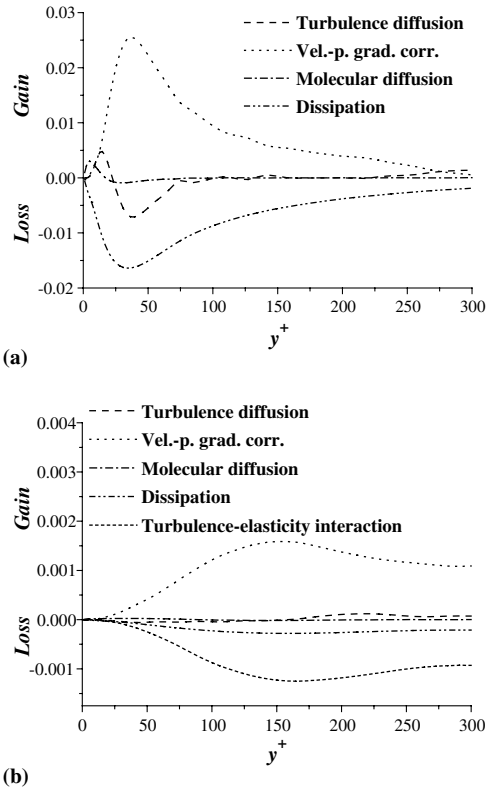

Fig. 11. Budget of Reynolds stress $\overline{v'^+v'^+}$: (a) Newtonian fluid and (b) surfactant solution.

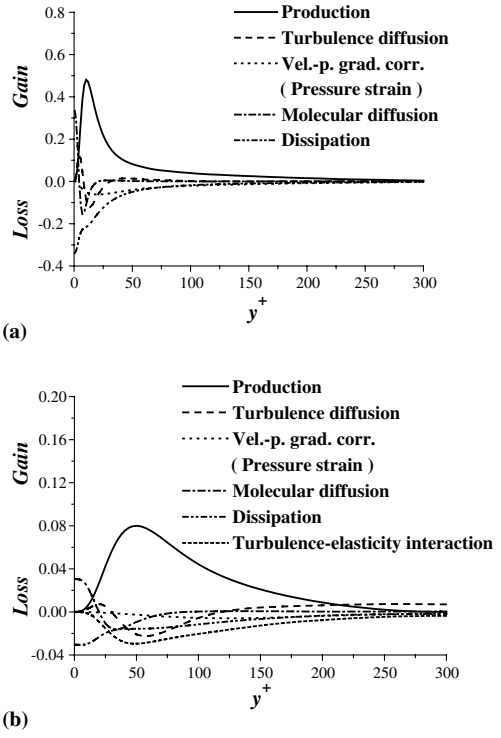

Fig. 10. Budget of Reynolds stress $\overline{u'^+u'^+}$: (a) Newtonian fluid and (b) surfactant solution.

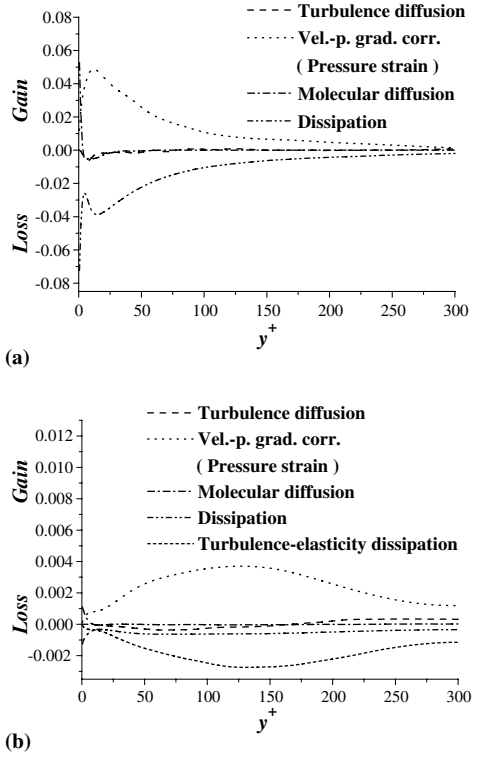

Fig. 12. Budget of Reynolds stress $\overline{w'^+w'^+}$: (a) Newtonian fluid and (b) surfactant solution.

With the addition of surfactant additives, the production is primarily lost by the turbulence–elasticity interaction term and the dissipation term. A very small amount of energy in the production rate is lost by the pressure strain. Thus, compared to the Newtonian fluid, the energy transferred from the $\overline{u'^+u'^+}$ to $\overline{v'^+v'^+}$ and $\overline{w'^+w'^+}$ becomes much smaller. Since the cross-flow gained less energy from the bulk flow, the velocity fluctuation in the wall-normal and spanwise directions decreases, resulting in weakened streamwise vortices. Fig. 13 compares the streamwise vortices in cross-section. With the addition of surfactant additives, the vortical structure becomes much larger and its strength becomes weaker. The violent streamwise vortices in the near wall region are significantly reduced and the vortical structures are evenly distributed in cross-section. The weakening of the streamwise vortices indicates that the additives significantly suppress the ejection and sweep motions occurring near the wall, which results in the suppressed turbulence production and Reynolds shear stress, indicating that the spacing between the high- and low-speed streaks becomes larger. Figs. 11 and 12 show that normal and spanwise velocity–pressure gradient correlations (no direct production term is available for $\overline{v'^+v'^+}$ and $\overline{w'^+w'^+}$, as the velocity–pressure gradient correlations are usually considered to be pseudo-productions) of surfactant solutions are less than one-tenth

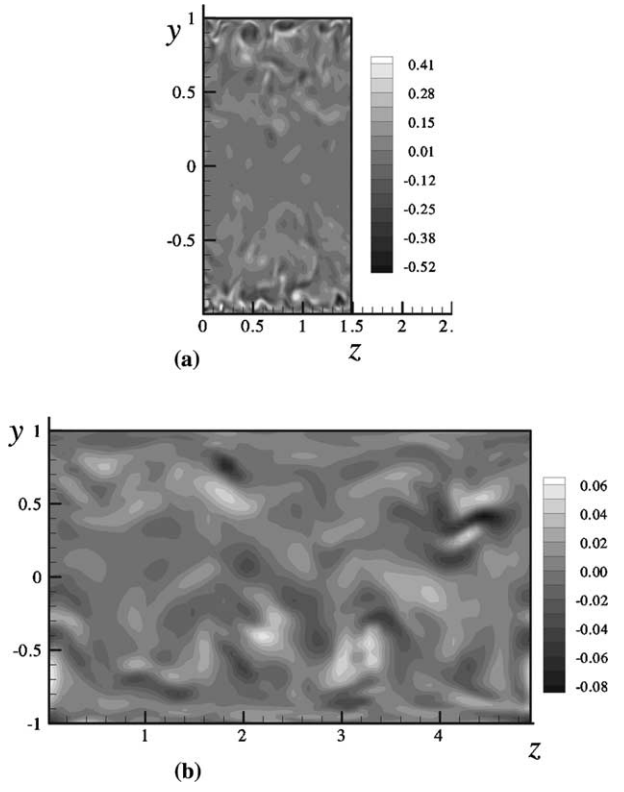

Fig. 13. Comparison of instantaneous streamwise vorticity for Newtonian flow and surfactant solution at a y–z cross-section: (a) Newtonian fluid and (b) surfactant solution.

of the values of the Newtonian fluid. Thus, v^+_{rms} and w^+_{rms} for the surfactant solutions decrease significantly as compared to the Newtonian fluid. The changes of the budget terms of the Reynolds normal stress $\overline{v'^+v'^+}$ and $\overline{w'^+w'^+}$ are flat, which explains the flat distribution of the v^+_{rms} and w^+_{rms} along the channel height (Fig. 5). The turbulent diffusion of $\overline{v'^+v'^+}$ for the surfactant solution becomes negligible, indicating that the turbulent transportation in the normal direction becomes very weak with the addition of the surfactant additives. In the Newtonian fluid, the dissipation terms are almost balanced with the velocity–pressure gradient terms in the budget of $\overline{v'^+v'^+}$ and $\overline{w'^+w'^+}$. With the addition of surfactant additives, however, the dissipation term becomes very small and the turbulence–elasticity interaction becomes a dominant dissipation term, to balance the velocity–pressure gradient term. All of these observations show that viscoelasticity plays an important role in the redistribution of the budget of Reynolds stress.

To our knowledge, this is the first report on the budget terms of Reynolds stress and kinetic energy of the viscoelastic fluid flow, using a Giesekus model. Previously, Dimitropoulos et al. (2001), Angelis et al. (2002), and Ptasinski et al. (2003) presented budget terms for a polymer solution by employing an FENE-P model. They found the viscoelastic contributions to be of a smaller magnitude with respect to the production and dissipation terms. For our study, the viscoelastic contribution term is of the same order of magnitude as the production term. The dissipation term becomes a smaller term in the budget of Reynolds normal stress $\overline{v'^+v'^+}$ and $\overline{w'^+w'^+}$. In addition, the magnitudes of the budget terms for our results are much smaller than those reported by Dimitropoulos et al. (2001), Angelis et al. (2002), and Ptasinski et al. (2003) and the peak value positions shifted further toward the bulk flow. The larger differences are the result of two factors, namely, the differences in the model and the computational parameters. In this study, the solution is more shear-thinning than the solutions used by Dimitropoulos et al. (2001), Angelis et al. (2002), and Ptasinski et al. (2003), which is a major factor causing the large differences in the redistribution of kinetic energy.

5. Discussion on uncertainty

In this section we analyze the uncertainty sources in the simulations. The uncertainty comes from both the simplified modeling of the network structures and numerical error. The poor quantitative agreement is primarily due to the Giesekus constitutive equation. We may choose other models, for example, FENE-P model or multimode model to improve the agreement. But we did not attempt to do it, because for the usage of any model, we need rheological data to obtain the model

parameters which cannot be precisely measured for dilute surfactant solution at the time being.

Another source of uncertainty is the numerical method. In this study we adopted a second-order finite difference scheme (Yu and Kawaguchi, 2004). The finite difference method has a lower-order accuracy than the spectral method. We employed this method rather than spectral method is because for spectral method, artificial terms have to be added in the constitutive equations to avoid numerical breakdown (Dimitropoulos et al., 1998). It is found the finite difference method proposed by Yu and Kawaguchi (2004) is more stable and accurate than the artificial spectral method. We believed once most of the smallest turbulence scales are solved, the resolution is acceptable. The grid and time resolutions of the present study were shown to be acceptable by comparing them with Kolmogorov scales.

The Kolmogorov length scale is

$$\eta^+ = \left(\frac{v^3}{\varepsilon}\right)^{1/4} \frac{U_\tau}{v} = \left(\frac{U_\tau^4}{\varepsilon v}\right)^{1/4} = \frac{1}{(\varepsilon^+)^{1/4}} \tag{19}$$

From the present simulation, ε^+ is seen to vary from 0.0159 near the wall to 0.00115 at the center of the channel (Fig. 9). Thus the Kolmogorov length scale in wall units has the smallest value of around 2.82 near the wall and the largest value of 5.43 at the center of the channel. The grid size in the wall-normal direction is smaller than in the Kolmogorov length scale at the near-wall region and comparable to the Kolmogorov length scale in the center region. In the streamwise and spanwise direction grids, sizes are larger than in the Kolmogorov length scale.

The Kolmogorov time scale in wall units is

$$t^+ = \left(\frac{v}{\varepsilon}\right)^{1/2} \frac{U_\tau^2}{v} = \frac{1}{(\varepsilon^+)^{1/2}} \tag{20}$$

It has the smallest value of 7.93 v/U_τ^2 near the wall and the largest value of 29.5 v/U_τ^2 at the center of the channel. The time step size used in the present study is 0.15 v/U_τ^2, which is much smaller than that of the Kolmogorov time scale. A more restrictive criterion for time increases requires the time-step size to be proportional to the time taken by a small-scale eddy passing a fixed point when advected by a macro-structure velocity, i.e., η^+/u^+. Our simulation also met this criterion. We must point out that the length scales are based on solvent viscosity. Also, since we know that the shear viscosity of the drag-reducing flow decreases with increases in the shear rate and finally reaches the viscosity of the solvent, a more suitable definition of length scale is based on the effective viscosity at the wall. Fig. 4 shows that the effective viscosity at the wall is 1.44 times larger than the solvent viscosity. Hence, the grid-spacings based on effective viscosity in the streamwise and spanwise directions are $\Delta x^+ = 12.8$ and $\Delta z^+ = 6.4$, respectively, and the grid-spacing Δy^+ varies from about 0.18 next to the wall to 3.7 in the center. These grid spacings are closer to those reported by Kim et al. (1987), who used $\Delta x^+ = 12$, $\Delta z^+ = 7$ and Δy^+, varying from about 0.05 to 4.4 for a Newtonian fluid.

In a word, as compared to the uncertainty of the model parameters, the uncertainty of numerical scheme is relatively small.

6. Conclusions

DNSs and experiments were performed for the fully developed turbulence flow of a Newtonian fluid and a 75 ppm CTAC surfactant solution in a channel. Realistic rheological properties were considered in the constitutive equations. The following conclusions can be drawn:

(1) Numerical results are in qualitatively agreement with the experimental data;
(2) Surfactant additives have dual effects on frictional drag to: (i) introduce positive mean viscoelastic shear stress, which has the function to increase frictional drag; and (ii) weaken the ejection and sweep events, to decrease frictional drag. The second effect is a major effect and thereby causes drag-reduction;
(3) Surfactant additives greatly alter the energy redistribution. Additives inhibit the input energy transfer from the mean flow to turbulent production, and inhibit the energy transfer from a streamwise velocity component to the wall-normal and spanwise velocity components. 64% of the energy supplied by the mean pressure gradient is dissipated to heat through the relaxation of the deformed network structures to their equilibrium state, and 36% of the energy is lost by viscosity and turbulent dissipation. The redistribution of energy due to elasticity changes leads to the lowered turbulence.

Acknowledgements

The authors thank Dr. Fukagata at Tokyo University for valuable discussion on FIK integration to identify the viscoelastic contribution to the frictional factors. This study was supported by the Ministry of Education, Culture, Sports, Science and Technology, through the project "Smart Control of Turbulence: A Millennium Challenge for Innovative Thermal and Fluids Systems, Japan."

References

De Angelis, E., Casciola, C.M., Piva, R., 2002. DNS of wall turbulence: dilute polymers and self-sustaining mechanisms. Comp. Fluids 31, 495–507.

De Gennes, P.G., 1990. Introduction to Polymer Dynamics. Cambridge University Press, Cambridge.

Dean, R.B., 1978. Reynolds number dependence of skin friction and other bulk flow variables in two-dimensional rectangular duct flow. Trans. ASME, J. Fluids Eng. 100, 215–223.

DenToonder, J.M.J., Hulsen, M.A., Kuiken, G.D.C., Nieuwstadt, F.T.M., 1997. Drag reduction by polymer additives in a turbulent pipe flow: numerical and laboratory experiments. J. Fluid Mech. 337, 193–231.

Dimitropoulos, C.D., Sureshkumar, R., Beris, A.N., 1998. Direct numerical simulation of viscoelastic turbulent channel flow exhibiting drag reduction: effect of the variation of rheological parameters. J. Non-Newton. Fluid Mech. 79, 433–468.

Dimitropoulos, C.D., Sureshkumar, R., Beris, A.N., Handler, R.A., 2001. Budgets of Reynolds stress, kinetic energy and streamwise enstrophy in viscoelastic turbulent channel flow. Phys. Fluids 13, 1016–1027.

Fukagata, K., Iwamoto, K., Kasagi, N., 2002. Contribution of Reynolds stress distribution to the skin friction in wall-bounded flows. Phys. Fluids 14 (11), L73–L76.

Kawaguchi, Y., Segawa, T., Feng, Z.P., Li, P.W., 2002. Experimental study on drag-reducing channel flow with surfactant additives—spatial structure of turbulence investigated by PIV system. Int. J. Heat Fluid Flow 23 (5), 700–709.

Kawaguchi, Y., Wei, J.J., Yu, B., Feng, Z.P., 2003. Rheological characterization of drag-reducing cationic surfactant solution—shear and elongational viscosities of dilute solutions. In: Proc. Fluids Engineering Division Summer Meeting, July 1–10, 2003, Honolulu, Hawaii.

Kim, J., Moin, P., Moser, R., 1987. Turbulence statistics in fully developed turbulent channel flow at low Reynolds number. J. Fluid Mech. 177, 133–166.

Lumley, J.L., 1969. Drag reduction by additives. Ann. Rev. Fluid Mech. 1, 367–384.

Lumley, J.L., 1973. Drag reduction in turbulent flow by polymer additives. J. Polym. Sci. 7, 263–290.

Min, T., Yoo, J.Y., Choi, H., Joseph, D.D., 2001. A role of elastic energy in turbulent drag reduction by polymer additives. Turbulence and Shear Flow Phenomena, Second International Symposium, KTH, Stockholm, 3, pp. 35–50.

Orlandi, P., 1995. A tentative approach to the direct simulation of drag reduction by polymers. J. Non-Newton. Fluid Mech. 60, 277–301.

Ptasinski, P.K., Boersma, B.J., Nieuwstadt, F.T.M., Vandenbrule, B.H.A.A., Hunt, J.C.R., 2003. Turbulent channel flow near maximum drag reduction: simulations, experiments and mechanism. J. Fluid Mech. 490, 251–291.

Sureshkumar, R., Beris, A.N., Handler, R.A., 1997. Direct numerical simulation of turbulent channel flow of a polymer solution. Phys. Fluids 9, 743–755.

Suzuki, H., Ishihara, K., Usui, H., 2001. Numerical study on a drag-reducing flow with surfactant additives. In: Proc. 3rd Pacific Rim Conference on Rheology.

Toms, B.A., 1948. Some observation on the flow of linear polymer solutions through straight tubes at large Reynolds numbers. In: Proc. 1st Int. Cong. Rheol., vol. 2. North Holland, Amsterdam, pp. 135–141.

Virk, P., Mickley, H., Smith, K., 1970. The ultimate asymptote and mean flow structure in Toms' phenomenon. ASME J. Appl. Mech. 37, 480–493.

Yu, B., Kawaguchi, Y., 2003. Effect of Weissenberg number on the flow structure: DNS study of drag-reducing flow with surfactant additives. Int. J. Heat Fluid Flow 24, 419–499.

Yu, B., Kawaguchi, Y., 2004. Direct numerical simulation of viscoelastic drag-reducing flow: a faithful finite difference method. J. Non-Newton. Fluid Mech. 116, 431–466.